

Electronic Supplementary Information

A global method for handling fluorescence spectra at high concentration derived from the competition between emission and absorption of colloidal CdTe quantum dots

Thomas Noblet, Laurent Dreesen, Julie Hottechamps and Christophe Humbert

- A. Processing of HR-TEM images
- B. Calculation of extinction cross sections
- C. Additional fluorescence spectra
- D. General method to process fluorescence spectra at high concentration
- E. Discussion about right angle, collinear and front-face configurations

A. Processing of HR-TEM images

Calculation of NC diameters. HR-TEM images exhibit diffraction patterns whose sizes directly correspond to those of NCs. In order to determine accurate values for the NC diameters of QD520 and QD610, we select only the diffraction patterns which are isolated enough. As shown in Figures A1 and A2, these patterns are delineated by circles on each image so that the measurements of their diameters with ImageJ (software that allows translating pixels into nanometers thanks to the scale) enable us to estimate a mean diameter for each kind of QD (i.e. QD520 and QD610). For both, we processed seven images for a total of 44 NCs selected. The associated statistical dispersions correspond to standard deviations.

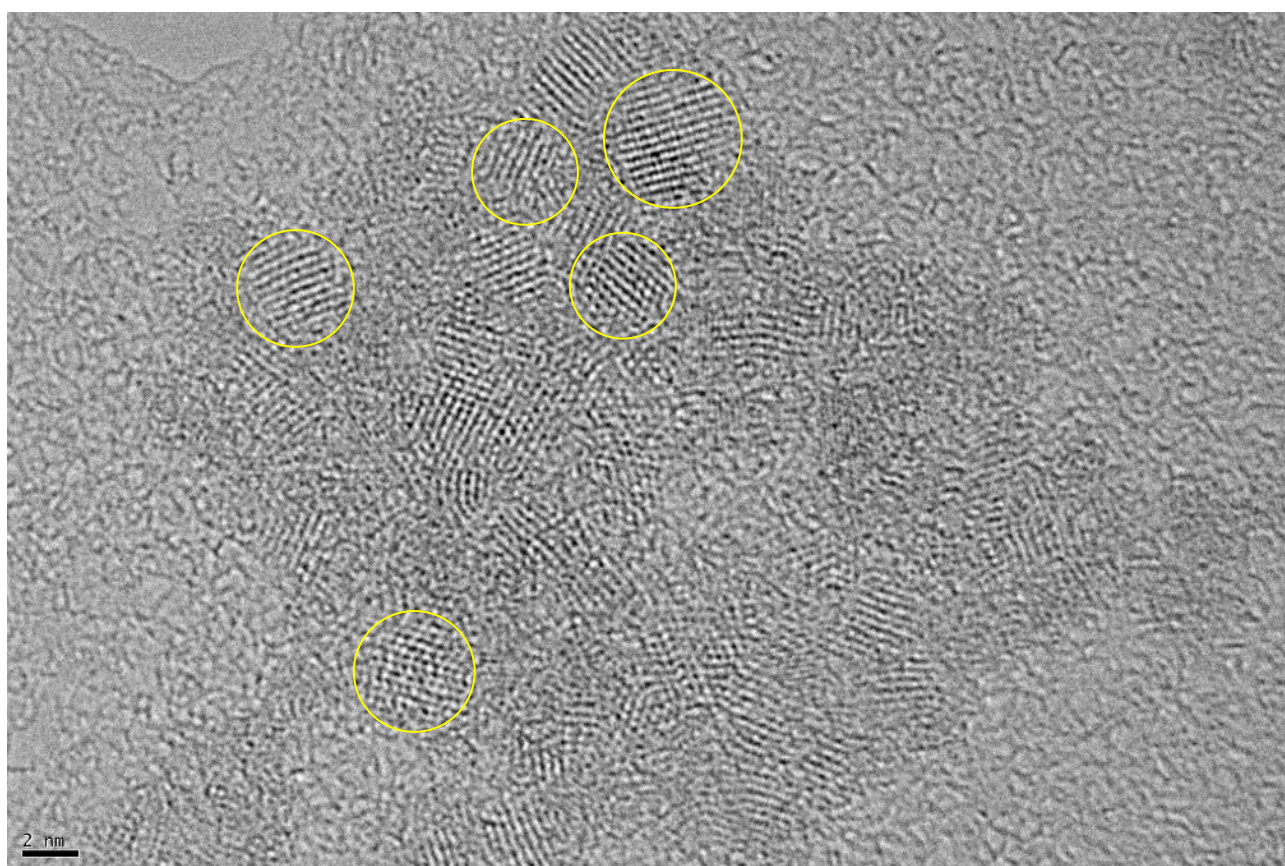


Figure A1 — Entire HR-TEM image associated to Fig. 2(a) for QD610.

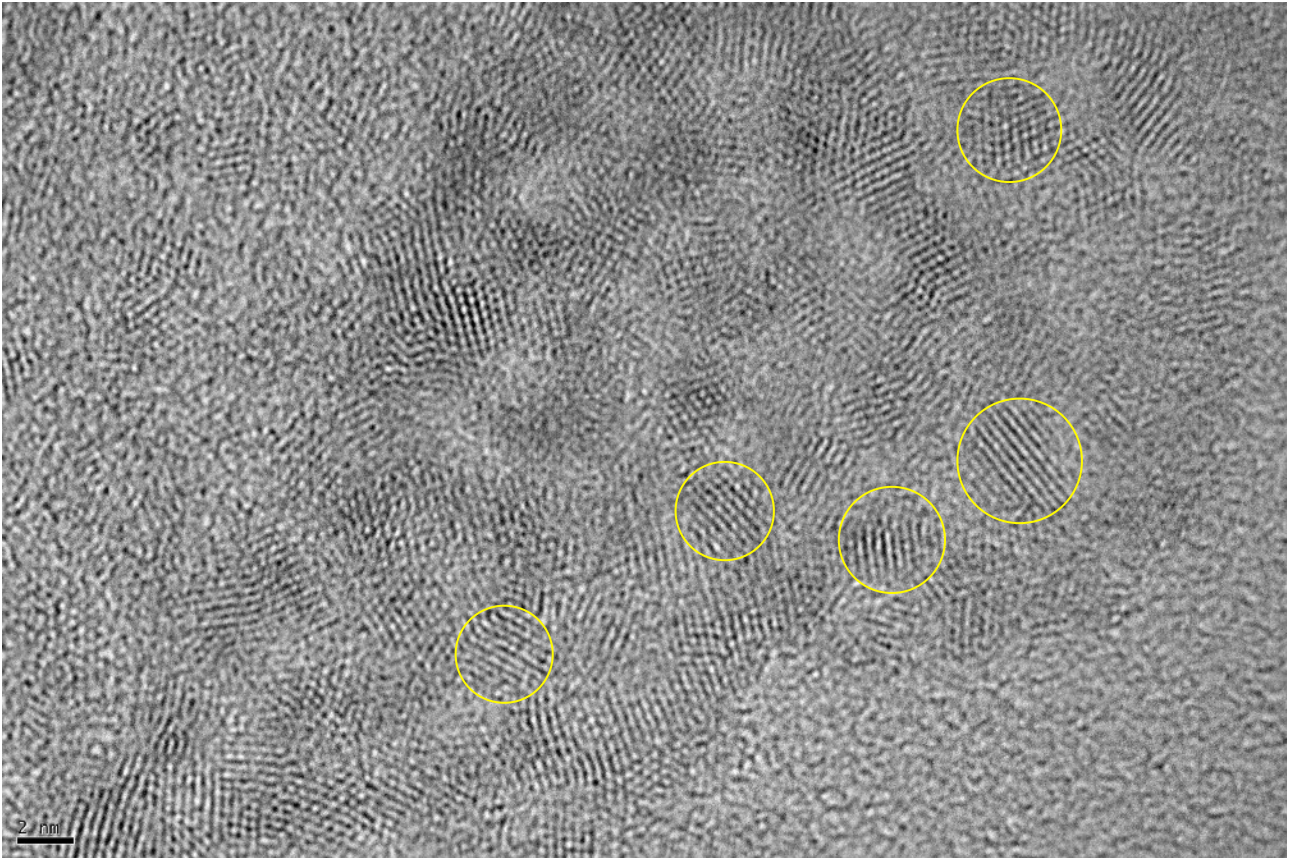


Figure A2 — Entire HR-TEM image associated to Fig. 2(a) for QD520.

Calculation of interplanar spacings. The d -spacings between reticular planes are calculated with two methods. The first one consists in drawing the profiles of lattice fringes along the directed lines $[uvw]$ associated to the planes (hkl) , as illustrated in Figure 2b. The second one is based on fast Fourier transform (FFT), computed with ImageJ. Table A summarizes the results and indicates for each value of d_{hkl} the method we used.

Planes (hkl)	$1/\sqrt{h^2+k^2+l^2}$	Average of $d(hkl)$	Standard deviation	Method
(111)	0.577	3.38	0.11	Profile
		3.29	0.12	FFT
		3.46	0.08	Profile
		3.42	0.13	FFT
(220)	0.354	2.05	0.05	FFT
		2.08	0.06	FFT
		2.08	0.20	Profile
(311)	0.302	1.74	0.05	FFT

Table A — Results obtained for the calculation of the interplanar spacings. The green cells correspond to QD520 and the red ones to QD610. Fig. 3b depicts the third column as a function of the second one.

Calculation of QD concentrations. The manufacturer data only specify the mass of CdTe, i.e. 25 mg for both QD520 and QD610. If it is easy to deduce the CdTe mass concentration (in g/L) according to the added volume of water, we need to use the structural properties of each type of QD (i.e. diameter and lattice parameter) to compute the concentrations in terms of QDs, instead of CdTe. Here we detail the steps of this calculation.

Let m be the mass of CdTe (in g) and V the added volume of water (in L). The CdTe mass concentration (in g/L) reads:

$$C_m(\text{CdTe}) = \frac{m}{V}.$$

In order to convert $C_m(\text{CdTe})$ into QD molar concentration, we calculate the number of CdTe atom-pairs per NC. Since there are 4 CdTe pairs in a unit cell, this number is given by:

$$n(\text{CdTe}/\text{QD}) = 4 \frac{\frac{4}{3}\pi \left(\frac{D}{2}\right)^3}{a^3} = \frac{2\pi}{3} \left(\frac{D}{a}\right)^3,$$

where D is the NC diameter and a the lattice parameter. The QD molar concentration (in M, i.e. mol/L) reads therefore:

$$C_M(\text{QD}) = \frac{C_m(\text{CdTe})}{\mathcal{M}(\text{CdTe}) \cdot n(\text{CdTe}/\text{QD})},$$

where $\mathcal{M}(\text{CdTe}) = 240.01$ g/mol is the molecular weight of CdTe. Last, the QD density (in m^{-3}) is given by:

$$N(\text{QD}) = C_M(\text{QD}) \cdot N_A \cdot 1000,$$

where N_A is the Avogadro constant.

B. Calculation of extinction cross section

The extinction cross section $\sigma(\lambda)$ of QDs is directly linked to their absorbance $\mathcal{A}(\lambda)$ thanks to the Beer-Lambert law:

$$\mathcal{A}(\lambda) = \frac{\sigma(\lambda) N \xi}{\ln 10} = \tilde{\sigma}(\lambda) N \xi,$$

where ξ is the length of the cuvette. To compute $\tilde{\sigma}(\lambda) = \sigma(\lambda)/\ln 10$, we can simply divide the absorbance $\mathcal{A}(\lambda)$ by N and ξ . However, to determine $\tilde{\sigma}(\lambda_{ex})$ at $\lambda_{ex} = 488$ nm as precisely as possible, we preferred to measure the absorbance (at 488 nm) for different QD concentrations. The extinction cross section thus derives from the linear regression of $\mathcal{A}(\lambda_{ex})/\xi$ with respect to N . The data are plotted in Figure B.

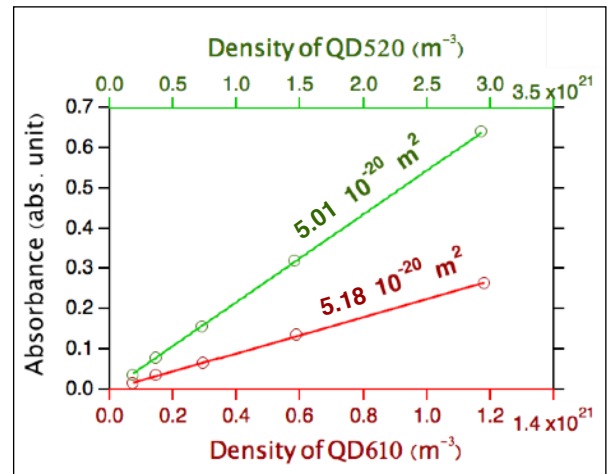


Figure B — Absorbance at 488 nm drawn with respect to QD density. The slopes of these curves give access to the extinction cross sections, here indicated in m^2 .

C. Additional fluorescence spectra

Figure 4 shows how the fluorescence intensity (Fig. 4a), the wavelength of maximum emission (Fig. 4b) and the spectral bandwidth (Fig. 4c) evolve with the QD concentration. Here, Figure C1 presents the fluorescence spectra from which Figure 4 derives. To insist on the spectral redshift and the decreasing of the bandwidth, the spectra are normalized and superimposed.

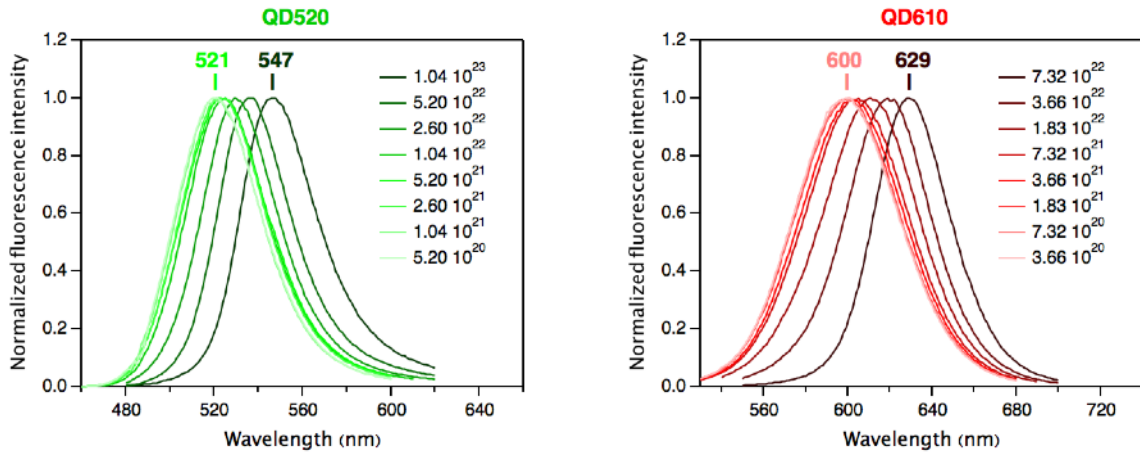


Figure C1 — Normalized fluorescence spectra of QD520 and QD610 at different concentrations. The legend indicates the respective QD densities in m^{-3} .

To show the accuracy of the model (that reveals especially useful at high concentration), we compare, in Figure C2, four experimental spectra with the corresponding modelings deduced from Equation (12).

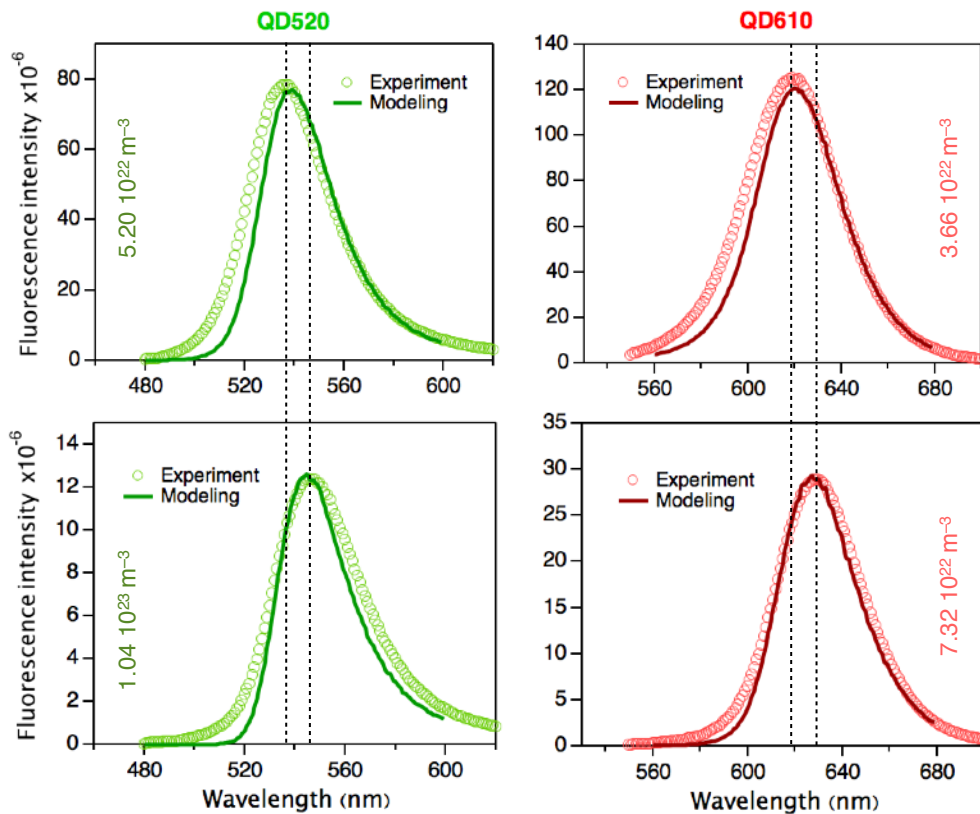


Figure C2 — Fluorescence spectra obtained for the two highest concentrations for each species (experimental curves) and their modelings.

D. General method to process fluorescence spectra at high concentration

Here we detail the global method to handle fluorescence spectra in the case of highly concentrated samples. We assume that the studied solution contains one fluorescent species, called f , and n other non-fluorescent chromophores, called C_i (where i describes the integers from 1 to n).

1 Computation of the extinction cross sections of all the species

First, to determine the extinction cross sections of the fluorophore f and the chromophores C_i , the easiest method consists in measuring their respective absorbances $\mathcal{A}_f(\lambda)$ and $\mathcal{A}_i(\lambda)$ over the spectral range of interest thanks to UV-visible spectroscopy in the case of solutions of which the densities (i.e. concentrations) N_f and N_i are known. The extinction cross sections $\tilde{\sigma}_f$ and $\tilde{\sigma}_i$ are then given as functions of the wavelength, according to:

$$\tilde{\sigma}_f(\lambda) = \frac{\mathcal{A}_f(\lambda)}{N_f \xi} \text{ and } \tilde{\sigma}_i(\lambda) = \frac{\mathcal{A}_i(\lambda)}{N_i \xi},$$

where ξ is the length of the cuvette.

2 Measurement of the reference fluorescence spectrum

Second, we need to measure the fluorescence spectrum of the fluorophore f in a solution wherein its concentration is low enough to be considered non-affected by inner filter effects. Obviously, it is much better if the fluorophore is the only species present in the solution. In the following, the reference fluorescence spectrum is called $F_0(\lambda_f)$ and the corresponding concentration $N_f^{(0)}$.

3 Prediction of the fluorescence spectrum at a given concentration

If you are interested in forecasting the fluorescence spectrum of the fluorophore f at a given concentration N_f in the presence of the n chromophores C_i (whose concentrations are N_i), you are henceforth able to use the generalized form of Eq.(12):

$$F(\lambda_f) = F_0(\lambda_f) \frac{N_f}{N_f^{(0)}} 10^{-\left(N_f - N_f^{(0)}\right)\left(\tilde{\sigma}_f(\lambda_{ex})\ell + \tilde{\sigma}_f(\lambda_f)L\right) - \sum_{i=1}^n N_i\left(\tilde{\sigma}_i(\lambda_{ex})\ell + \tilde{\sigma}_i(\lambda_f)L\right)},$$

where ℓ and L are the parameters defined in Fig. 1. If the concentration N_f is unknown, you can use this equation to fit with the experimental spectrum and then deduce N_f .

4 Correction of a fluorescence spectrum at a given concentration

To reconstruct the real fluorescence spectrum $\tilde{F}(\lambda_f)$ from $F(\lambda_f)$, you need to compute:

$$\tilde{F}(\lambda_f) = F(\lambda_f) 10^{N_f\left(\tilde{\sigma}_f(\lambda_{ex})\ell + \tilde{\sigma}_f(\lambda_f)L\right) + \sum_{i=1}^n N_i\left(\tilde{\sigma}_i(\lambda_{ex})\ell + \tilde{\sigma}_i(\lambda_f)L\right)}.$$

E. Discussion about right angle, collinear and front-face configurations

In this article, we acquired the fluorescence spectra in right angle geometry (Fig. 1 and Figure E1-a). From a physical and conceptual point of view, the equations presented in the paper and generalized in ESI, section D, remain applicable in the cases of other geometric configurations. In Figure E1-b, we give the example of the collinear configuration. In both cases, the parameters ℓ and L describe respectively the pathlengths of (i) the incident beam and (ii) the fluorescence emission collected by the spectrometer.

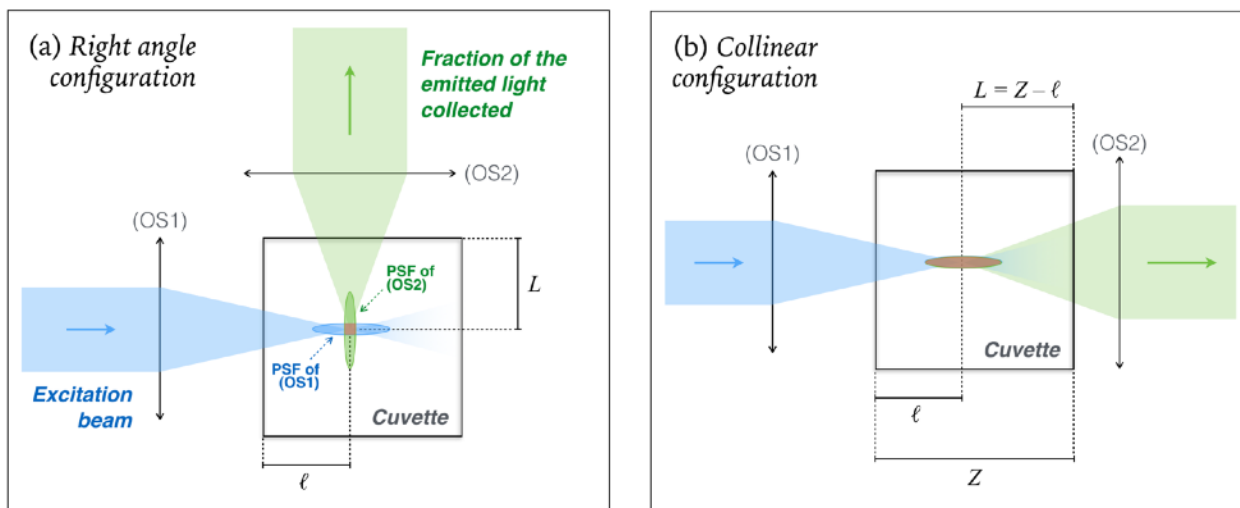


Figure E1 — Sketch and principle of (a) the right angle configuration and (b) the collinear configuration. (OS1) depicts the optical system which focuses the excitation beam and (OS2) is the optical system which collects the emitted light. The oval areas represent the point spread functions (PSF) of the two. Their intersection is colored in red.

Unlike the right angle configuration, the collinear geometry implies a relation between ℓ and L . Indeed, their sum corresponds to the length Z of the cuvette ($\ell + L = Z$), so that the fitting procedure only requires one of the two parameters. Although this relation may constitute an advantage for fitting the measurements in the collinear case, the right angle geometry is proper to study *independently* the PIFE (directly related to ℓ) and the SIFE (related to L), whereas it is not possible in collinear configuration. Moreover, given the common oblong shape of the point spread functions (PSF) which limit the spatial resolution of the optical systems (microscope objectives, typically) used in spectrometers (Figure E1), the geometric parameters ℓ and L are quite better defined in the case of the right angle configuration. As illustrated in Figure E1-a, the intersection between the PSFs of the two optical systems, in right angle configuration, can be considered as a point: the measurements are then sensitive to the inner filter effects *at that point* (assumption on which our model is based). In collinear geometry, we actually observe the inner filter effects at several points distributed along the Z -direction. As a result, our correction method may be less appropriate in that case.

For the interested reader, a general discussion about the influence of common sample geometries on the observation of inner filter effects is provided by J. R. Lakowicz [*Instrumentation for Fluorescence Spectroscopy*, in *Principles of Fluorescence Spectroscopy*, Springer, 2006]. In particular, this shows experimentally how crucial inner filter effects are in right angle geometry, and how negligible they are in front-face configuration (Figure E2).

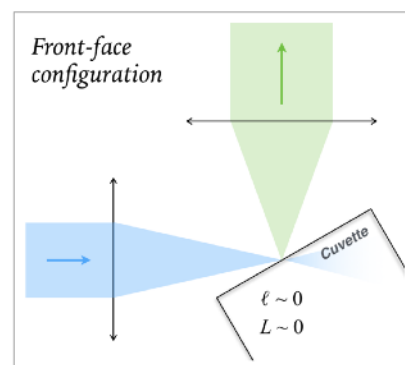


Figure E2 — Sketch of the front-face configuration.